The Company of Biologists

RESEARCH ARTICLE

CFAP157 is a murine downstream effector of FOXJ1 that is specifically required for flagellum morphogenesis and sperm motility

Marina Weidemann[1], Karin Schuster-Gossler[1], Michael Stauber[1], Christoph Wrede[2], Jan Hegermann[2], Tim Ott[3], Karsten Boldt[4], Tina Beyer[4], Katrin Serth[1], Elisabeth Kremmer[5], Martin Blum[3], Marius Ueffing[4] and Achim Gossler[1],*

ABSTRACT

Motile cilia move extracellular fluids or mediate cellular motility. Their function is essential for embryonic development, adult tissue homeostasis and reproduction throughout vertebrates. FOXJ1 is a key transcription factor for the formation of motile cilia but its downstream genetic programme is only partially understood. Here, we characterise a novel FOXJ1 target, *Cfap157*, that is specifically expressed in motile ciliated tissues in mouse and *Xenopus* in a FOXJ1-dependent manner. CFAP157 protein localises to basal bodies and interacts with tubulin and the centrosomal protein CEP350. *Cfap157* knockout mice appear normal but homozygous males are infertile. Spermatozoa display impaired motility and a novel phenotype: *Cfap157*-deficient sperm exhibit axonemal loops, supernumerary axonemal profiles with ectopic accessory structures, excess cytoplasm and clustered mitochondria in the midpiece regions, and defective axonemes along the flagella. Our study thus demonstrates an essential sperm-specific function for CFAP157 and suggests that this novel FOXJ1 effector is part of a mechanism that acts during spermiogenesis to suppress the formation of supernumerary axonemes and ensures a correct ultrastructure.

KEY WORDS: Cfap157, Ciliogenesis, Axoneme, Spermiogenesis, Male infertility

INTRODUCTION

Motile cilia are slender protrusions of the surface of eukaryotic cells. Their core, the axoneme, consists of nine peripheral microtubular doublets and typically two central microtubules. The axoneme carries dynein arms and originates at the basal body, a centriolar structure anchored to the cell cortex. Motile cilia move extracellular fluids, mediate cellular motility and play essential roles during development, tissue homeostasis and reproduction (reviewed by Choksi et al., 2014b; Gerdes et al., 2009; Nigg and

[1]Institute for Molecular Biology, OE5250, Hannover Medical School, Carl-Neuberg-Str. 1, Hannover 30625, Germany. [2]Institute of Functional and Applied Anatomy, OE8840, Hannover Medical School, Carl-Neuberg-Str. 1, Hannover 30625, Germany. [3]Institute of Zoology, University of Hohenheim, Garbenstraße 30, Stuttgart 70593, Germany. [4]Institute of Ophthalmic Research, Center for Ophthalmology, University of Tübingen, Röntgenweg 11, Tübingen 72076, Germany. [5]Institute of Molecular Immunology, Helmholtz Zentrum München, German Research Center for Environmental Health (GmbH), Core Facility Monoclonal Antibodies, Marchioninistr. 25, München 81377, Germany.

*Author for correspondence (gossler.achim@mh-hannover.de)

A.G., 0000-0002-9103-9116

Raff, 2009). In vertebrate embryos, motile cilia in the left-right organiser rotate and generate a leftward flow of the extracellular fluid, which is translated into left-right asymmetry of visceral organs (reviewed by Blum et al., 2014; Nonaka et al., 1998; Takeda et al., 1999). Coordinated beating of motile cilia on epithelia of the lung is required for airway clearance (Jain et al., 2010; Stannard and O'Callaghan, 2006). Motile cilia on ependymal cells lining the brain ventricles secure normal cerebrospinal fluid flow (Banizs et al., 2005; Jacquet et al., 2009; Lee, 2013; Spassky et al., 2005) and motile cilia in the fallopian tube contribute to movement of eggs (Lyons et al., 2006). Motility of the sperm flagellum is essential for sperm function (Afzelius and Eliasson, 1983). Consequently, human primary ciliary dyskinesia (PCD), which is caused by dysfunction of motile cilia, is associated with situs randomisation, respiratory problems, male infertility and, less frequently, with female infertility and hydrocephalus (reviewed by Praveen et al., 2015).

Whereas cells of respiratory epithelia and ependyma form multiple motile cilia, spermatozoa carry one flagellum, a specialised motile cilium with specific accessory structures. The flagellum consists of: the connecting piece, which links it to the sperm head and holds the centriole from which the axoneme nucleates; the midpiece, which contains nine outer dense fibres (ODFs) and peripheral mitochondria; the principal piece, which possesses both ODFs and a peripheral fibrous sheath; and the end piece (reviewed by Eddy, 2006). The flagellum develops during differentiation of spermatids in seminiferous tubules of testes. Concomitantly, the sperm head reshapes and the acrosome, which is a sperm-specific secretory vesicle, forms (reviewed by Fléchon, 2016). Most of the cytoplasm is removed via a residual body that detaches from the neck region and, via a cytoplasmic droplet that is shed at the midpiece-principal piece boundary, the annulus (reviewed by Hermo et al., 2010). Spermatozoa are stored in the cauda epididymis, where they undergo further maturation (reviewed by Buffone et al., 2012; Cornwall, 2009).

FOXJ1 is a key transcription factor for the formation of motile cilia throughout vertebrates (Alten et al., 2012; Brody et al., 2000; Chen et al., 1998; Stubbs et al., 2008; Vij et al., 2012; Yu et al., 2008). FOXJ1 targets include: structural, motor and accessory proteins of the axoneme; intraflagellar and vesicular transport proteins; and basal body components (reviewed by Santos and Reiter, 2008). Additional proteins are thought to be involved in the function of cilia (Andersen et al., 2003; Gerdes et al., 2009; Gherman et al., 2006; McClintock et al., 2008). Comparing the transcriptomes of fetal respiratory epithelia before and after motile ciliogenesis, and heterozygous with homozygous *Foxj1* mutant

DEVELOPMENT

lungs, we identified a few hundred candidates for FOXJ1 effectors during ciliogenesis. Here, we describe the analysis of one candidate, *Cfap157*, that encodes a basal body protein of unknown function. *Cfap157* transcription correlates with the presence of motile cilia and depends on FOXJ1. Despite its expression in many cell types with motile cilia, loss of *Cfap157* function in mice specifically affects flagellum morphogenesis and sperm motility.

RESULTS

Expression and localisation of *Cfap157*

Cfap157 (GeneID 227736) encodes a 523 amino acid protein that lacks known motifs, except for a PEST domain (http://bioinf.cs.ucl.ac.uk/psipred/), is conserved among chordates and shares sequence identity of variable extent with proteins of various other eukaryotes, including the green algae *Chlamydomonas* (Table S1). Mouse *Cfap157* expression detected by RT-PCR was essentially confined
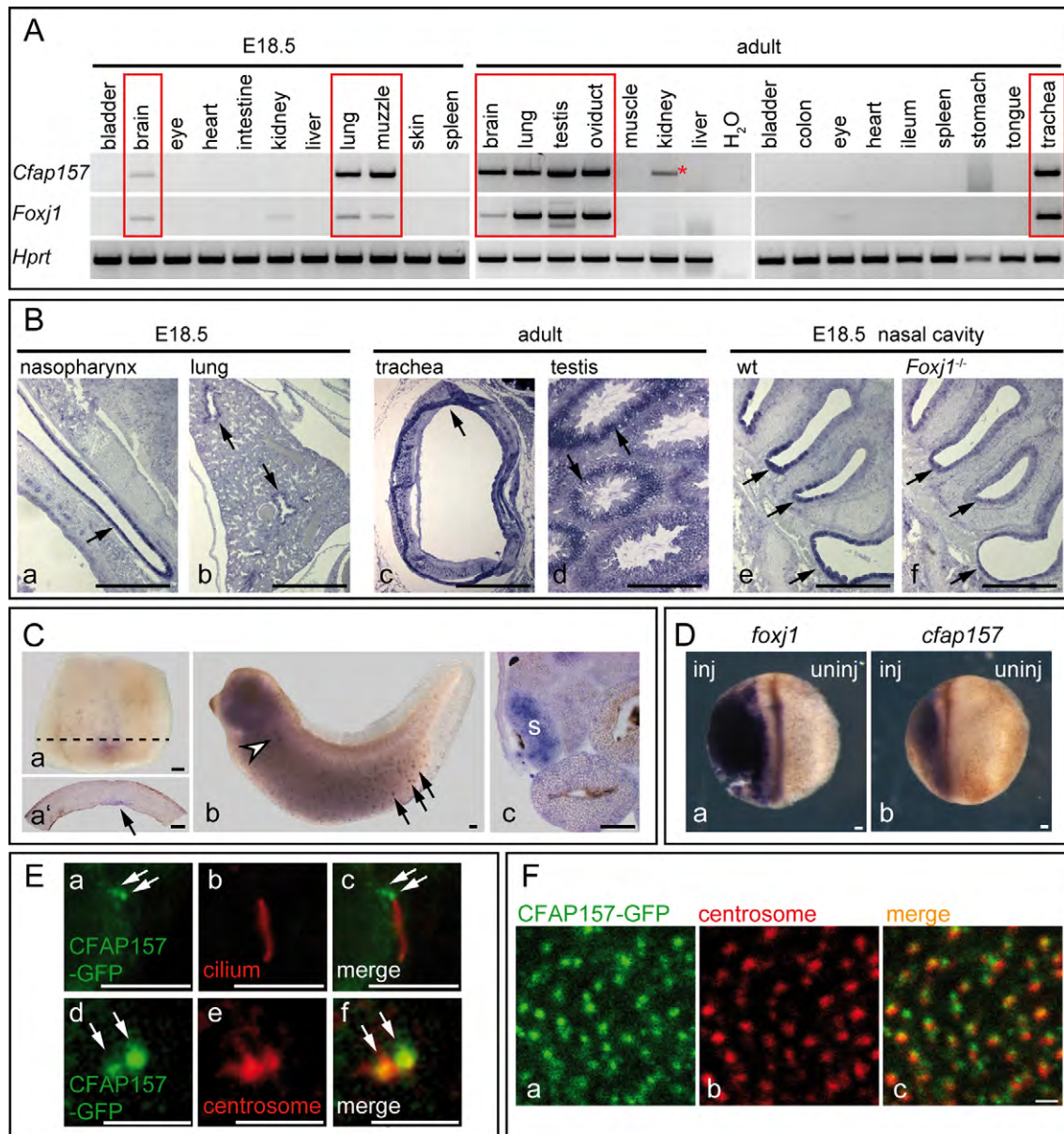

Fig. 1. Expression and localisation of *Cfap157* RNA and protein. (A) RT-PCR with primers in exons 1 and 3 of *Cfap157*, in exons 2 and 3 of *Foxj1*, and in exons 7 and 9 of *Hprt* on RNA isolated from E18.5 and adult wild-type mouse tissues. Boxes indicate co-expression of *Cfap157* and *Foxj1* in tissues carrying motile cilia. Asterisk indicates *Cfap157* PCR product in kidney that was not consistently detected by RT-PCR (see Fig. 3D). (B) Section *in situ* hybridisation with a full-length *Cfap157* cDNA probe on E18.5 and adult wild-type mouse tissues, as well as E18.5 *Foxj1* wild-type (wt) and *Foxj1*-deficient (*Foxj1*^{−/−}) sagittal nose sections. Arrows indicate expression domains. Scale bars: 500 µm in a-c,e,f; 250 µm in d. (C) Whole-mount *in situ* hybridisation of *Xenopus laevis* embryos with a full-length *cfap157* cDNA probe at stage 16 (a, dorsal explant; a′, transverse section along plane shown in a; arrow, gastrocoel roof plate), stage 35 (b; arrowhead, nephrostomes; arrows, multiciliated epidermal cells) and stage 45 (c; transverse section of tadpole; s, stomach). Scale bars: 100 µm. (D) Whole-mount *in situ* hybridization with a full-length cDNA *foxj1* probe (a) or a *cfap157* probe (b) on stage 20 *Xenopus* embryos after left-sided injection of *foxj1* mRNA (*n*=37). Scale bars: 100 µm. (E) Localisation of CFAP157-GFP protein at the basal body of IMCD3 cells co-stained with acetylated tubulin (a-c) or γ-tubulin (d-f). Arrows, CFAP157-GFP. Scale bars: 5 µm in a-c; 2 µm in d-f. (F) Localisation of CFAP157-GFP protein to basal bodies of motile cilia on cells of stage 30 *Xenopus* larval epidermis co-stained with γ-tubulin. Scale bar: 1 µm.

to tissues containing motile cilia correlating with the expression of *Foxj1* (Fig. 1A, boxes). Section *in situ* hybridisation showed *Cfap157* expression in epithelia known to carry motile cilia and spermatogenic cells in testes (Fig. 1Ba-d, arrows). *Cfap157* was downregulated in airway epithelial cells of *Foxj1*-null mutants (Fig. 1Be,f, arrows), confirming that *Cfap157* transcription depends on FOXJ1 in these cells. Whole-mount *in situ* hybridisation of *Xenopus* embryos revealed *cfap157* (GeneID 780234) expression in cells carrying motile cilia (Fig. 1C). Consistent with the transcriptional dependence of *Cfap157* on FOXJ1 in mice, overexpression of *foxj1* induced ectopic expression of *cfap157* in *Xenopus* embryos (Fig. 1D).

We analysed the subcellular localisation of CFAP157 in inner medullary collecting duct 3 (IMCD3) cells, which express endogenous *Cfap157* and form non-motile cilia, by expressing GFP fusions (because our anti-CFAP157 antibodies did not detect endogenous CFAP157). In IMCD3 cells induced to form cilia CFAP157-GFP was enriched in two adjacent dots near the ciliary base (Fig. 1Ea-c) that co-stained with γ-tubulin (Fig. 1Ed-f), indicating localisation at the basal body. Consistently, GFP-labelled CFAP157 expressed in *Xenopus* embryos showed multiple dots subapical to the membrane that overlapped with γ-tubulin in multiciliated epidermal cells, also indicating localisation to basal bodies of motile cilia (Fig. 1F).

Identification of potential protein interaction partners of CFAP157

To identify interaction partners of CFAP157, SF-TAP-tagged (Gloeckner et al., 2007) full-length CFAP157 or CFAP157ΔPEST (lacking the C-terminal PEST domain) was expressed in HEK293T cells and purified by Strep-FLAG tandem affinity purification. The eluates were analysed by liquid chromatography fractionation and mass spectrometry (LC-MS). Interesting candidate interaction partners in HEK293T cells included the two tubulins TUBA4A and TUBB5, basigin, and the centrosomal proteins CEP350 and SSNA1 (Table S2). SSNA1 was also significantly enriched among proteins pulled down from testis lysates using purified SF-TAP-tagged CFAP157ΔPEST, in addition to various other proteins (Table S3). Co-immunoprecipitation assays using CHO cells co-expressing full-length HA-tagged CFAP157ΔPEST and myc- or flag-tagged versions of potential interaction partners thus far confirmed the interaction of CFAP157 with TUBA4A, TUBB5 and CEP350 (Fig. 2A, boxes) but not with basigin and SSNA1. Assays using HA-tagged full-length CFAP157, which is expressed at lower levels than the ΔPEST-version, produced similar results (data not shown). A direct or indirect interaction of CFAP157 with tubulins and CEP350 is consistent with the localisation of CFAP157 at ciliary basal bodies and with the co-expression of *Cfap157* and *Cep350* in brain, lung and testis (Fig. 2B).

Generation of *Cfap157*^{*lacZ*} and *Cfap157*^{Δex2} knockout mice

To analyse the physiological function of CFAP157, we generated mutant mice (Fig. 3A) using the EUCOMM ESC clone G05 (*1700019L03Rik*^{*tm1a(EUCOMM)Hmgu*}) and validated them using PCR and Southern blot analysis (Fig. 3B,C). In these mice, a *lacZ* gene and a *neo* cassette were inserted into intron 1, and exon 2 was flanked by loxP sites (*Cfap157*^{*lacZneo*}). Additional loxP and FRT sites allowed for removal of *neo* and exon 2 to generate a null allele with a *lacZ*-reporter (*Cfap157*^{*lacZ*}) or for removal of *lacZ* and *neo* to generate a conditional allele (*Cfap157*^{*ex2flox*}). Deletion of exon 2 (*Cfap157*^{Δex2}) causes a frameshift and termination of translation in
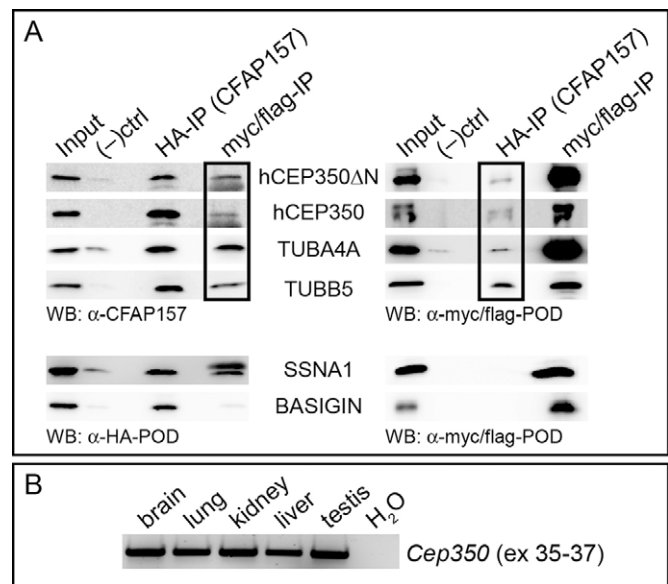

Fig. 2. Analysis of putative CFAP157 protein interaction partners identified by tandem affinity purification/mass spectrometry (TAP/MS). (A) Co-immunoprecipitation (IP) of HA-CFAP157ΔPEST and myc- or flag-tagged potential interaction partners: myc-hCEP350; myc-hCEP350ΔN (Yan et al., 2006); TUBA4A-flag; TUBB5-flag; SSNA1-flag; BASIGIN-myc; (−)ctrl, IP performed without antibodies. CO-IP bands are boxed. (B) *Cep350* RT-PCR on RNA isolated from adult mouse tissues; H₂O, control without cDNA.

exon 3 and/or nonsense-mediated mRNA decay. These alleles were generated using Zp3-Cre (de Vries et al., 2000) or flp-deleter mice (Rodríguez et al., 2000) and verified by using PCR.

Homozygous *Cfap157*^{*lacZ*} or *Cfap157*^{Δex2} mice were born at Mendelian ratios (Table S4) and were indistinguishable from wild-type mice. *Cfap157* transcripts were not detected in RNA from homozygous brain and lung (Fig. 3D, Fig. S1). However, RT-PCR on testis RNA of homozygous *Cfap157*^{Δex2} mice amplified fragments of transcripts lacking either exon 2 or both exon 2 and exon 3 (Fig. 3E, asterisk and arrowhead), which is probably caused by alternative splicing and stabilisation of mRNA that can occur during spermatogenesis due to removal of destabilising 3′UTR sequences (Kleene, 2005; Li et al., 2016). The latter transcript could be translated into a CFAP157 protein lacking 142 amino acids. qRT-PCR suggested significant expression of this transcript (Fig. S2). However, northern blot analysis with a full-length *Cfap157* cDNA probe detected no transcripts in *Cfap157*^{*lacZ*} and *Cfap157*^{Δex2} testis RNA (Fig. 3F). Importantly, no CFAP157 protein could be precipitated from homozygous *Cfap157*^{*lacZ*} and *Cfap157*^{Δex2} testis lysates (Fig. 3G, arrowheads and bracket; direct detection of CFAP157 in lysates using western blots was precluded by high background) using antibodies raised against peptides encoded by exons 1 and 7. These results demonstrated that *Cfap157*^{*lacZ*} and *Cfap157*^{Δex2} are null alleles.

Analysis of reporter expression in *Cfap157*^{*lacZ*} mice and dependence of *Cfap157* transcription on FOXJ1

β-Galactosidase staining of *Cfap157*^{*lacZ*} embryonic and fetal tissues revealed *lacZ* expression in the node of E8 embryos, in the fourth ventricle of the brain at E12.5 and in the airways at E18.5 (Fig. 4A, arrows). In adults, *lacZ* was expressed in the airways of the lung, the ependymal layer of the ventricles and the seminiferous tubules of testis (Fig. 4B). On a *Foxj1*-null background (Brody et al., 2000), reporter expression from the *Cfap157*^{*lacZ*} allele was lost (e.g. fetal
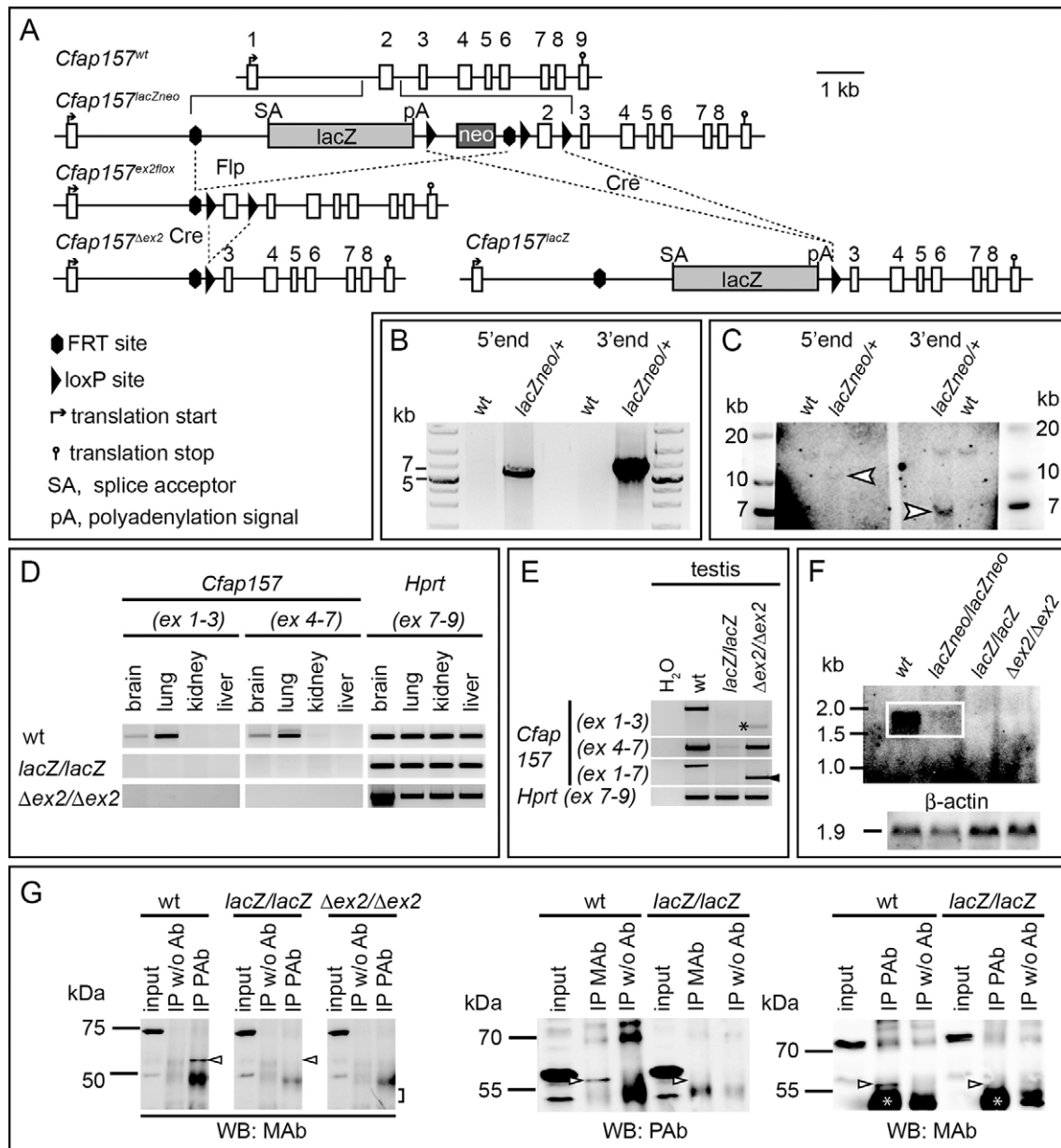
Fig. 3. Generation and verification of *Cfap157* knockout mice. (A) Targeting strategy. (B) Validation of targeting by LR-PCR at the 5′ and 3′ end of the integrated transgene performed with wild-type (wt) and *Cfap157*^{lacZneo/+} genomic DNA. (C) Southern blot analysis with external 5′ and 3′ probes on wild-type and *Cfap157*^{lacZneo/+} genomic DNA; arrowheads, expected transgenic signals. (D) RT-PCR with primers binding in *Cfap157* exons 1 and 3, *Cfap157* exons 4 and 7, and *Hprt* exons 7 and 9 of on RNA from adult tissues (for complete gel photos, see Fig. S4). (E) RT-PCR with primer pairs as in D and a pair binding in *Cfap157* exons 1 and 7 on adult testes RNA (asterisk and arrowhead, sequenced Δex2 and Δex2,3 products, respectively). H₂O, control without cDNA. (F) Northern blot analysis of testis RNA probed with full-length *Cfap157* cDNA; box, signal at the expected size. The faint wild-type signal obtained for *Cfap157*^{lacZneo/lacZneo} suggested read-through transcription and splicing around the lacZ/neo cassette (Fig. S3). Homozygous *Cfap157*^{lacZneo} mice displayed both *lacZ* reporter expression and full male fertility. Bottom, same northern blot re-probed with β-actin. (G) Immunoprecipitation of CFAP157 from wild-type or *Cfap157* mutant testis lysates using polyclonal (PAb) or monoclonal (MAb) antibodies. IP w/o Ab, negative control without antibody; arrowheads, CFAP157; bracket, expected position of CFAP157^{Δex2,3} (44 kDa) (all CFAP157 signals were detected slightly below the expected size); asterisks, immunoglobulin heavy chain.

lungs, Fig. 4Ce,f; node, Fig. S4), corroborating the observation that FOXJ1 is an essential transcriptional activator of *Cfap157*.

Essential function of *Cfap157* restricted to male fertility

Analysis of inner organs revealed no situs defects in heterozygous and homozygous *Cfap157*^{lacZ} (*n*=177 and 76) and *Cfap157*^{Δex2} mice (*n*=37 and *n*=22). In addition, we observed no hydrocephalus, renal cysts (Fig. 5A) or mucus accumulation in nasal cavities (Fig. 5Ba,b, circles) in *Cfap157* mutants. Light and transmission

electron microscopy (TEM) showed no differences between cilia in homozygous *Cfap157*^{lacZ} and wild-type lung epithelia (Fig. 5Bc-h). Likewise, histological analysis of homozygous *Cfap157*^{lacZ} oviducts and testes revealed no differences to wild type or heterozygotes (Fig. 5C).

Homozygous *Cfap157*^{lacZ} and *Cfap157*^{Δex2} females were fertile and gave rise to litters of normal size (Table S5). By contrast, homozygous males carrying either allele were infertile. They left vaginal plugs in timed matings (8/8 *Cfap157*^{lacZ} and 4/4
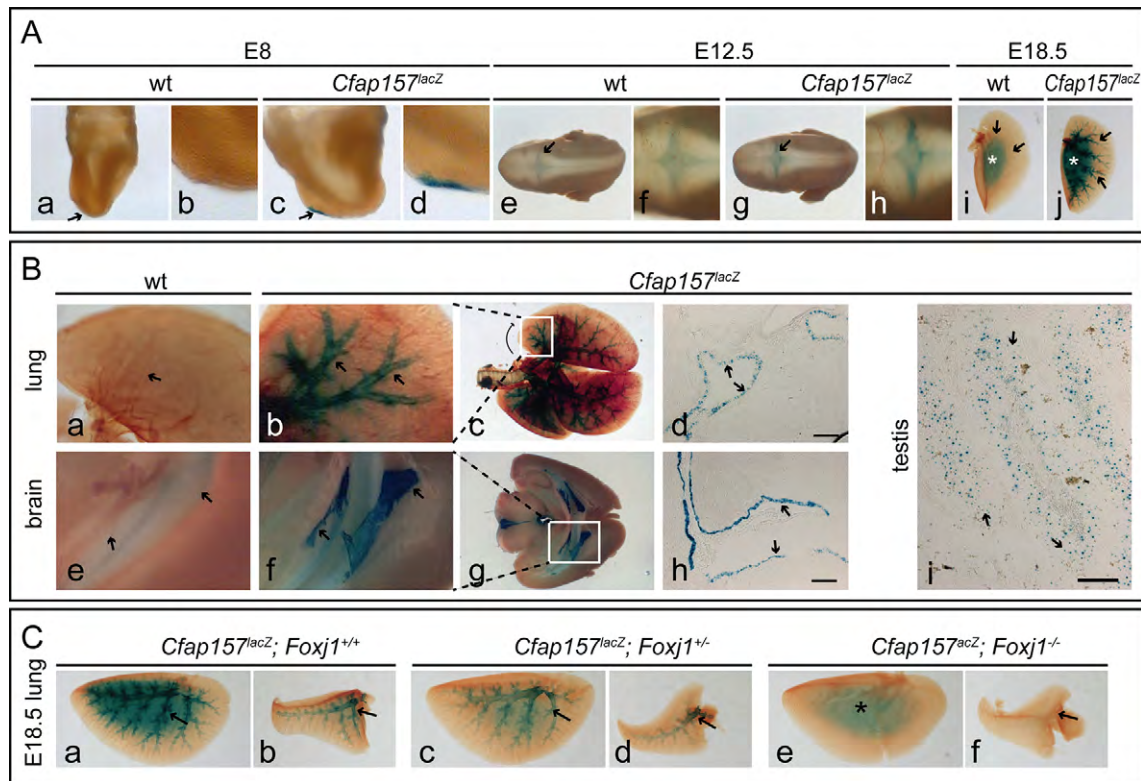
Fig. 4. FOXJ1-dependent reporter expression in *Cfap157^lacZ* mice. (A) *lacZ* expression in *Cfap157^lacZ* E8 (a-d) and E12.5 (e-h) embryos, and E18.5 lungs (i,j). (B) *lacZ* expression in *Cfap157^lacZ* adult lung (b-d), brain (f-h) and testis (i); wild type (wt; a,e), negative control. Lungs were cleared with benzyl alcohol:benzyl benzoate (a-c). (d,h,i) Cryosections. (b,f) Higher magnifications of boxed areas in c,g. Scale bars: 100 μm in d,h,i. (C) β-Galactosidase expression in E18.5 lung lobes of *Cfap157^lacZ* mice that were *Foxj1^+/+* (a,b; *n*=4), *Foxj1^+/−* (c,d; *n*=2) or *Foxj1^−/−* (e,f; *n*=5). Arrows indicate the node (in Aa,c), ventricle/ependyma (in Ae,g, Be-h), airways (in Ai,j, Ba-d,Ca-d,f) or spermatogenic cells (Bi). Asterisks indicate background staining.

Cfap157^Δex2 homozygous males) but never generated pregnancies. In addition, continuous matings (3-5 months) with homozygous *Cfap157^lacZ* (*n*=16) or *Cfap157^Δex2* (*n*=7) males produced no offspring. Collectively, these analyses indicated a CFAP157 function that is distinctly required for sperm function.

Cfap157 functions in sperm motility and flagellum morphogenesis

Cfap157 mutant sperm dissected from the cauda epididymis ('cauda sperm') displayed a reduced and abnormal motility, often resulting in twitching or local circular movement (Movies 1 and 2). Most *Cfap157* spermatozoa contained a bulge in the proximal flagellum next to a dislocated head (see below). Computer assisted sperm analysis (CASA; Yániz et al., 2015) of *Cfap157* mutant cauda sperm showed a severely reduced motility rate (Fig. 6A, Table S6) and a significantly lower concentration (Fig. 6B, Table S6).

Cauda sperm of 4- to 6-month-old *Cfap157* mutant males bound eggs inefficiently and hardly moved them, in contrast to wild-type sperm (Fig. 6C, *n*>12 eggs; Movies 3 and 4). *In vitro* fertilisation (IVF) assays showed that *Cfap157* mutant sperm are essentially unable to fertilise eggs even when in close contact: 143/211 (68%) wild-type eggs incubated with sperm from fertile heterozygous *Cfap157^lacZ/+* males developed pronuclei, indicating fertilisation, whereas only 13/488 (2.7%) wild-type eggs incubated with sperm from homozygous *Cfap157^lacZ/lacZ* males were fertilised (Table S7). Likewise, the development of blastocysts occurred in only 4/1111 (0.4%) and 1/810 (0.1%) wild-type eggs incubated with cauda sperm from *Cfap157^lacZ/lacZ* and *Cfap157^Δex2/Δex2* males,

respectively, whereas incubation with wild-type sperm produced blastocysts in 260/437 (58%) eggs (Fig. 6D, Table S8). As IVF with both wild-type and mutant sperm resulted in a lower percentage of blastocysts than fertilised eggs, the loss of embryos appears unrelated to the CFAP157 mutation.

Staining various structures in cauda sperm of ∼6-month-old *Cfap157* mutant males revealed morphological abnormalities in the midpiece region in 95% of sperm cells that were identical for both alleles (*n*=125 *Cfap157^lacZ*; *n*=129 *Cfap157^Δex2* spermatozoa; Fig. 7A-E). Ninety-three percent (235/254) of sperm cells showed an axonemal loop of the midpiece (Fig. 7Ac,d,g,h, Bc,d,g,h) and 6% (14/254, some also with a loop) contained a bulge (Fig. 7Ae,f). Seventy-five percent (191/254) of sperm heads were bent abnormally (Fig. 7Ac,g, Bc,g) and 12% (31/254) were missing (Fig. 7Be). The loop appeared to contain excess cytoplasm (Fig. 7Ac,g, Bc,g). Haematoxylin and Eosin staining of *Cfap157* sperm cells confirmed that surplus cytoplasm incorporated the loop completely in some, and partially in other spermatozoa (not shown). Co-staining of the annulus at the midpiece–principal piece boundary using anti-septin 7 antibodies revealed that the axonemal loop was restricted to the midpiece (*n*=45; Fig. 7Bd,f,h). Staining of acetylated tubulin showed that 76/180 spermatozoa contained a connecting microtubular link that appeared to fix the loop (Fig. 7Bd,h, arrows). The rest did not show such a link, perhaps obscured by twisted or narrow loops (Fig. 7Ad,h). Staining with AKAP3 antibodies showed the presence of ectopic fibrous sheath in the midpiece region close to the sperm head in 111/139 spermatozoa (arrows and arrowheads in Fig. 7Cd,f,h) and much less in the principal piece. Ten out of 139 mutant sperm cells had no AKAP3-
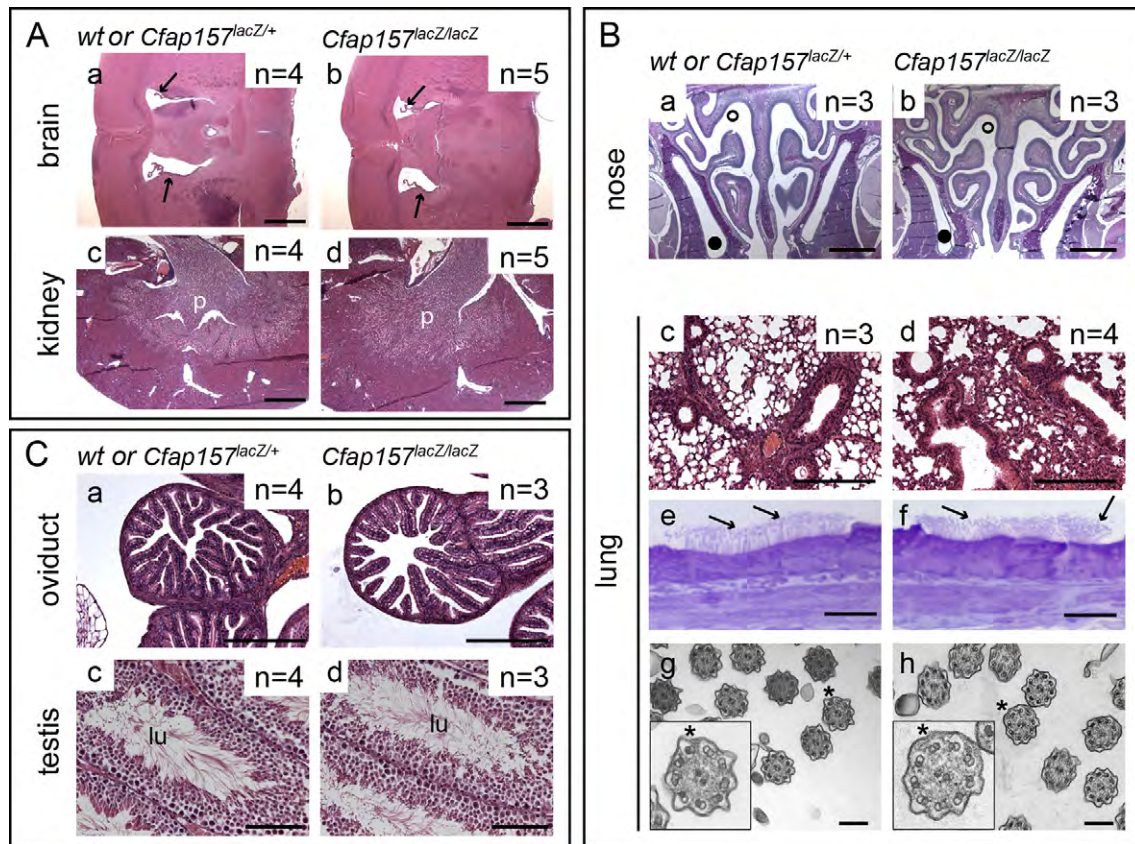
Fig. 5. *Cfap157^lacZ/lacZ* tissues without phenotypic alteration. (A) HE-stained adult brain (a,b; coronal sections; arrows, lateral ventricles) and kidney (c,d; p, renal pelvis; one homozygous kidney completely sectioned to check for micro-cysts but none were found). Arrows indicate ventricles. (B) Periodic acid-Schiff (PAS) staining of coronal nose sections (a,b; open circle, lumen; filled circle, sinus), HE-stained lung sections (c,d), light microscopy of thin lung sections (e,f; arrows, cilia), TEM of pulmonary cilia (g,h; asterisks, axonemal profiles magnified in insets). (C) HE-stained oviduct (a,b) and testis sections (c,d; lu, lumen of seminiferous tubule). Scale bars: 1 mm in A; 1 mm in Ba,b; 250 μm in Bc,d and Ca,b; 10 μm in Be,f; 200 nm in Bg,h; 100 μm in Cc,d.

labelled fibrous sheath, and 18/139 looked like wild-type sperm, which contained fibrous sheath exclusively in the principal piece (n=34; Fig. 7Cb). Staining with MitoTracker revealed an accumulation of mitochondria near the axonemal link but not along the axoneme of the looped midpiece (n=75; Fig. 7Dd). The length of the looped midpiece (*Cfap157^lacZ/lacZ*, 23±1 μm, n=6; *Cfap157^Δex2/Δex2*, 23±1 μm, n=17; *Cfap157^lacZ /+*, 23±1 μm, n=8) and of the remaining flagellum (*Cfap157^lacZ/lacZ*, 94±7 μm, n=16; *Cfap157^Δex2/Δex2*, 93±4 μm, n=13; *Cfap157^lacZ /+*, 93±4 μm, n=6) was similar to wild type and consistent with previous wild-type measurements (Cummins and Woodall, 1985). Nuclei (n=147) and acrosomes (n=65) of *Cfap157* sperm stained with DAPI and lectin appeared normal (Fig. 7Ab,d,f,h). Collectively, these analyses show that CFAP157 is required for the normal organisation of the midpiece axoneme, for the transport/localisation of the fibrous sheath and mitochondria, as well as for elimination of excess cytoplasm, processes that occur in the seminiferous tubules prior to spermiation. CFAP157 is absent from epididymal sperm (Fig. S5), perhaps reflecting the disintegration of centrioles in mature sperm (Eddy, 2006) or the overall loss of proteins during sperm maturation (Skerget et al., 2015). This indicates that CFAP157 is no longer present in mature sperm and supports a function exclusively in the testis.

To monitor the development of the *Cfap157* phenotype in testes, we analysed sections of seminiferous tubules at all stages of spermatogenesis, which we identified by the size and shape of

acrosomes and nuclei (Ahmed and de Rooij, 2009; Meistrich and Hess, 2013) that were indistinguishable between wild type and *Cfap157* mutants (n=3) at all stages (total of 246 mutant tubule sections). Consistent with previous observations (Zhang et al., 2012), mitochondria (stained using anti-COX IV antibodies) aligned in wild-type midpieces of spermatids beginning at stage 14/15 (arrowheads in Fig. 8Aa,a′,b,b′; Fig. S6Ac,c′) and formed slender threads projecting from the sperm heads into the lumen at stage 16 (arrowheads in Fig. 8Ac,c′; Fig. S6Ad-g,d′-g′). As in wild type, *Cfap157*-null tubules displayed aligned mitochondria beginning at stage 14/15 (arrowheads in Fig. 8Ad-f′; Fig. S6An,n′). At stage 16, mitochondrial threads appeared less regular, partly kinky and bulky (arrows Fig. 8Af,f′; Fig. S6Ar,r′), and sperm heads lining the lumen were not well oriented (Fig. 8Af,f′; Fig. S6Ao-r, o-r′). There was no evidence for the strong accumulation of mitochondria observed in cauda sperm (Fig. 7), suggesting that clustering of mitochondria occurs after spermiation. Prior to stage 12, the fibrous sheath marker AKAP3 was diffusely distributed in the cytoplasm of developing spermatids. As previously described (Sakai et al., 1986), fibre-like structures appeared first in spermatids at stage 13 (arrows in Fig. S6Ba,a′,l,l′) and were prominent thereafter (arrows in Fig. 8Ba,a′,c,c′). Fibres were present at a distance from the sperm heads in mature wild-type sperm (Fig. 8Bc,c′; Fig. S6Bg,g′), resulting in a zone devoid of AKAP3 staining between the sperm heads lining the lumen and the principal pieces (arrowheads in Fig. 8B; Fig. S6Bf,f′,g,g′). By
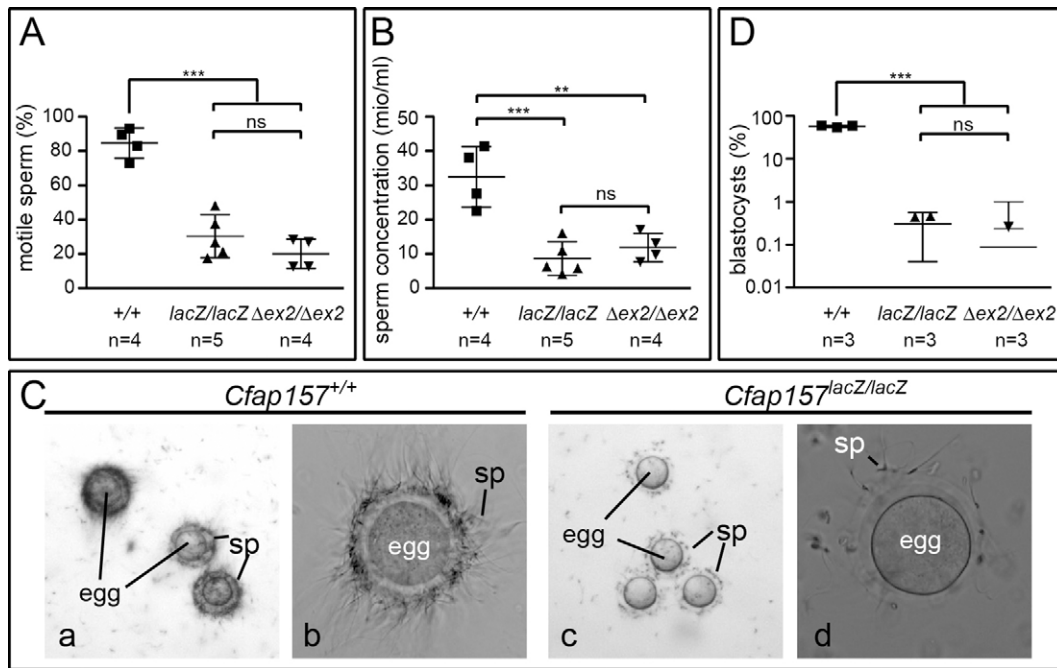
Fig. 6. Motility and fertility of *Cfap157* sperm. (A,B) Analysis of motility (A) and sperm number (B) of wild-type, homozygous *Cfap157^(lacZ/lacZ)* and *Cfap157^(Δex2/Δex2)* cauda sperm isolated from adult mice (>2 months old). (C) Pictures taken from Movies 3 and 4 performed during IVF of wild-type eggs with wild-type (a,b) and *Cfap157^(lacZ/lacZ)* (c,d) sperm (sp). (D) Percentage of wild-type eggs that developed into blastocysts after IVF with wild-type or mutant sperm [logarithmic scale; three data points (zero values) are not shown]. Data are mean±s.d.; ns, not significant; **$P<0.01$; ***$P<0.001$; *n*, number of males analysed.

contrast, fibrous, dotted and diffuse AKAP3 staining in *Cfap157* mutant sperm was found in abnormal positions and in the vicinity of sperm heads (asterisks in Fig. 8Bd,d′-f,f′; Fig. S6Bn-r,n′-r′), suggesting that ectopic accumulation of fibrous sheaths develops during late stages of spermiogenesis.

Ultrastructural defects in CFAP157-deficient sperm

TEM of *Cfap157^(lacZ/lacZ)* cauda epididymis sections showed fewer sperm in the mutant than in the wild type (Fig. 9A) and expanded structures probably representing the abnormal *Cfap157*-null midpieces observed by light microscopy (Fig. 9Ab, blue arrows). Cell membranes around some of these structures were fragmented (Fig. 9Ab, yellow arrow), indicating reduced stability.

Longitudinal sections of *Cfap157^(lacZ/lacZ)* sperm (Fig. 9Ca,b,g) revealed a dislocated sperm head (bent by 180° in Fig. 9Ca) and a large cytoplasmic remnant (arrow). Although microtubule fibres were not visible in this section, ODFs continuous in midpiece branches and the principal piece (Fig. 9Cb, arrows; Fig. S7Ae,f) suggested the fusion of two midpiece axonemes to form a single principal piece axoneme, i.e. an axonemal fork. The axonemal loop, visible by the ODFs, ran along the edge of the cell, encircling the excess cytoplasm (Fig. 9Cg, arrow).

Cfap157^(lacZ/lacZ) midpiece regions contained irregular arrangements of mitochondria clustered around a central axonemal profile (Fig. 9Cc; stars, red arrow) and additional peripheral axoneme profiles (Fig. 9Cc, yellow arrows) that were surrounded by a fibrous sheath (Fig. 9Cd, hexagon) consistent with the enrichment of fibrous sheath in the midpieces of isolated cauda sperm (Fig. 7C). Peripheral axonemes were not surrounded by individual plasma membranes and are therefore unlikely to represent sections through folded or clustered flagella. The presence of similar groups of peripheral axonemes on opposite sides of the cell implied that bundles of a varying number of

axonemes formed the axonemal loops, consistent with the lack of mitochondria attached to them (Fig. 7Dd, Fig. 9Cc,d).

Finally, we observed defective axonemes in *Cfap157* mutant sperm missing or displaying dislocated microtubule doublets at various flagellar levels [compare Fig. 9Bc,d with 9Cc,d,f (arrowheads) and Fig. 9Be with 9Ce (arrowheads); Fig. S7] in about one out of three mutant axoneme profiles. Profiles of coupled axonemes confirmed the presence of axoneme bundles in *Cfap157* mutant sperm (Fig. 9Cf). The mirror image of the incomplete axonemes and ODFs of this example (Fig. 9Cf, arrowheads and asterisks) suggested that both profiles belonged to the same folded axoneme. Defective axonemes typically possessed a central microtubule pair, suggesting that they were assembled incompletely rather than split after assembly, although we cannot exclude other mechanisms. Microtubules of mutant axonemes possessed inner and outer dynein arms (Fig. S8), indicating that *Cfap157* is not required for dynein arm assembly.

DISCUSSION

We identified *Cfap157* from microarray screens of FOXJ1-dependent genes in the mouse fetal lung (Stauber et al., 2016). *Cfap157* also appeared in several other screens that suggested activation by FOXJ1 (Choksi et al., 2014a), involvement in ciliogenesis (Hoh et al., 2012; Ivliev et al., 2012; McClintock et al., 2008) and association with human PCD (Geremek et al., 2011, 2014). Here, we show that CFAP157 is a novel FOXJ1 effector that is expressed in various motile ciliated tissues but essential only during spermatogenesis.

Cfap157: a FOXJ1 target with a sperm-specific function

Cfap157 expression correlated with *Foxj1* expression and the presence of motile cilia in mouse and frog, and endogenous *Cfap157* expression in mice depended on FOXJ1. Despite its
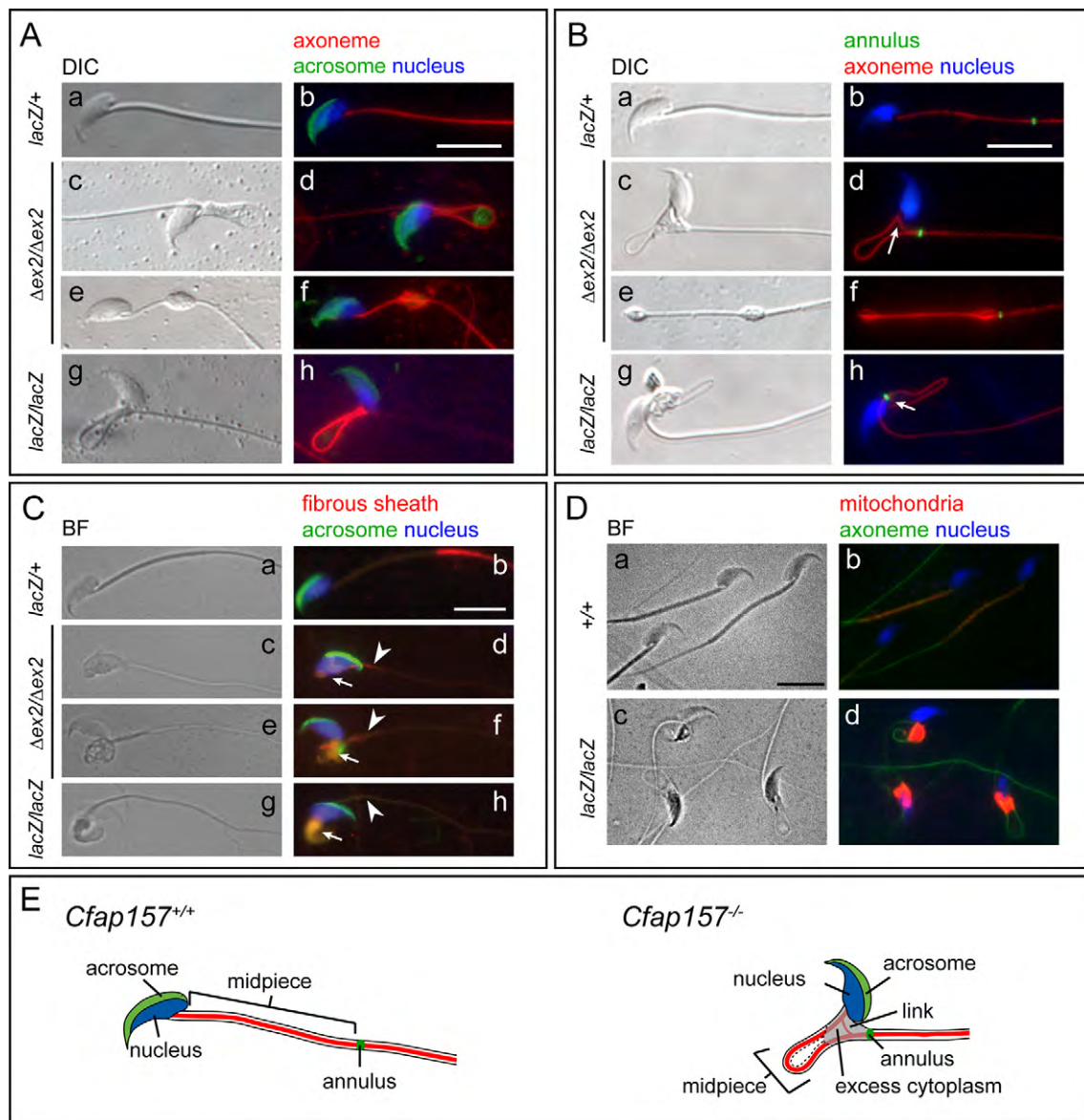
Fig. 7. Phenotypic analysis of *Cfap157* mutant sperm. (A) Cauda sperm from *Cfap157^lacZ/+* (a,b), *Cfap157^Δex2/Δex2* (c-f) and *Cfap157^lacZ/lacZ* (g,h) mice stained for axonemes (red), nuclei (blue) and acrosomes (green). (B) Sperm of the same genotypes as in A stained for axonemes (red), nuclei (blue) and annuli (green); arrows indicate axonemal linker at the base of the midpiece loop. (C) Sperm of the same genotypes as in A stained for fibrous sheaths (red), nuclei (blue) and acrosomes (green); arrows indicate abnormal localisation of fibrous sheath material close to the sperm head; arrowheads indicate straight midpiece region. (D) Wild-type and *Cfap157^lacZ/lacZ* sperm stained for mitochondria (red), nuclei (blue) and axonemes (green). (E) Schematic drawing depicting the *Cfap157* phenotype observed by immunocytochemistry; fibrous sheath and mitochondria are not shown (compare with D). DIC, differential interference contrast; BF, bright field. Scale bars: 10 µm.

expression in several tissues, both mutant *Cfap157* alleles specifically affected only the formation and function of the sperm flagellum, although we cannot rule out minor defects in other motile cilia without obvious functional consequences. Possibly, CFAP157 function is compensated for in some motile cilia after gene disruption, as described in *Cep131* mutant mice (Hall et al., 2013) and in zebrafish mutants (Rossi et al., 2015). However, the identity of any compensating factor remains undetermined and it appears plausible that the sperm flagellum with its unique accessory structures has requirements that differ from other motile cilia. This presumption is supported by mutations of other ciliogenesis factors that distinctly affect sperm cells: e.g. disruption of *Spef2* causes disorganised flagellar axonemes and male infertility but normal tracheal axonemes (Sironen et al., 2011). In contrast to *Cfap157*,

Spef2-deficient mice still exhibit sinusitis and hydrocephalus, putatively due to a reduction of the beat frequency of the respective motile cilia (Sironen et al., 2011). Conservation of mouse and human CFAP157 protein (Table S1) suggests that human CFAP157 may play a similar role in male fertility and that mutations would result in a similar phenotype.

A unique sperm phenotype in *Cfap157* mutants
Impaired sperm motility, reduced sperm numbers and inefficient attachment of mutant spermatozoa to the zona pellucida (collectively observed in all 13 *Cfap157^lacZ/lacZ* and 8 *Cfap157^Δex2/Δex2* males analysed) can be explained by the expanded and disorganised midpiece and dislocated head, supernumerary axonemes and a disrupted axonemal arrangement.
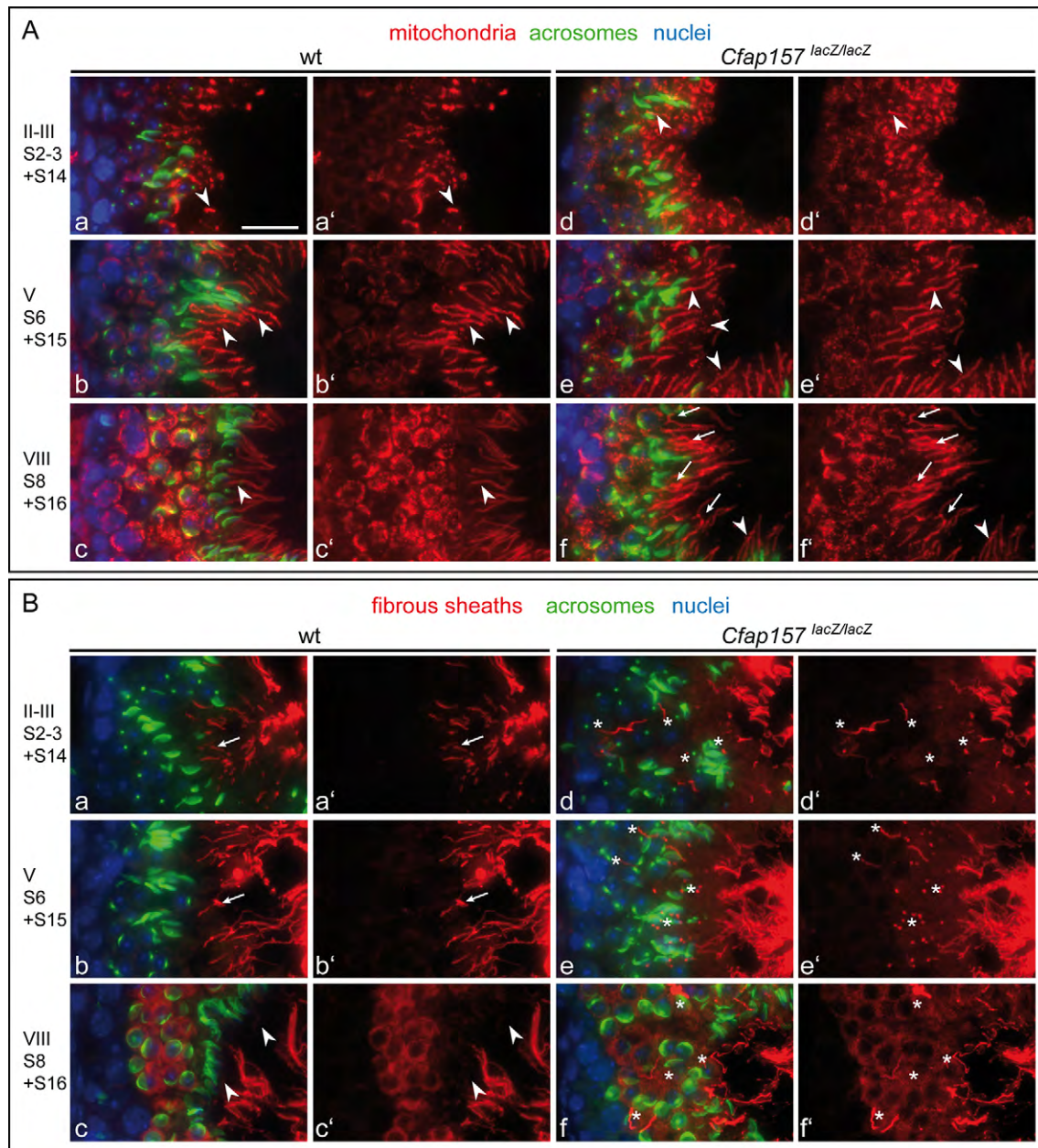
Fig. 8. Phenotypic analysis of *Cfap157* mutant testes. Sections of wild-type (Aa-c′,Ba-c′) and *Cfap157^lacZ/lacZ* mutant (Ad-f′,Bd-f′) testes stained for acrosomes (green) and nuclei (blue), and (A) mitochondria (red; 155 analysed mutant tubule sections) or (B) fibrous sheaths (red; 91 analysed mutant tubule sections). Roman numbers indicate the stage of the epithelial cycle; arabic numbers indicate the stage of spermatogenesis. (A) Arrowheads indicate mitochondria aligning in threads; arrows indicate abnormally arranged mitochondria. (B) Arrows indicate forming fibres; arrowheads indicate normal midpiece regions devoid of fibrous sheath; asterisks indicate abnormally located fibrous sheath material. Scale bars: 25 μm. Lumen is towards the right.

Cfap157-deficient sperm heads are bent with respect to the flagellar axis; consequently, flagellar beating does not drive spermatozoa into the egg but along the surface, away from the egg. This and sterical hindrance may have caused the reduced binding to eggs and the failure to penetrate the zona pellucida that requires the impetus of the sperm (Buffone et al., 2012). The reduced sperm concentration is unlikely to contribute to infertility because a similar reduction in sperm numbers in *Arl4*-null mice did not affect fertility (Schürmann et al., 2002).

The most peculiar aspect of the phenotype was the looped axoneme in the disorganised midpiece region containing multiple axonemal profiles. The additional axonemal profiles could be derived either from ectopic nucleation of several axonemes or

from fragmented or broken axonemes. However, tubulin staining showed continuous axonemes throughout the flagellum (e.g. Fig. 7A,B,D) and localisation of CFAP157 to basal bodies would be consistent with a centriolar function, arguing in favour of ectopic nucleation. Fibrous sheath normally occurs only in the principal piece and its formation progresses from distal to proximal up to the annulus (Irons and Clermont, 1982). The presence of fibrous sheath around *Cfap157*-deficient midpiece axonemes suggests that an apparently normal annulus may not be sufficient to prevent the formation of fibrous sheath in the midpiece. Immunocytochemical analysis suggested that the abnormal distribution of fibrous sheath occurs during late stages of spermiogenesis and that mitochondrial clustering develops
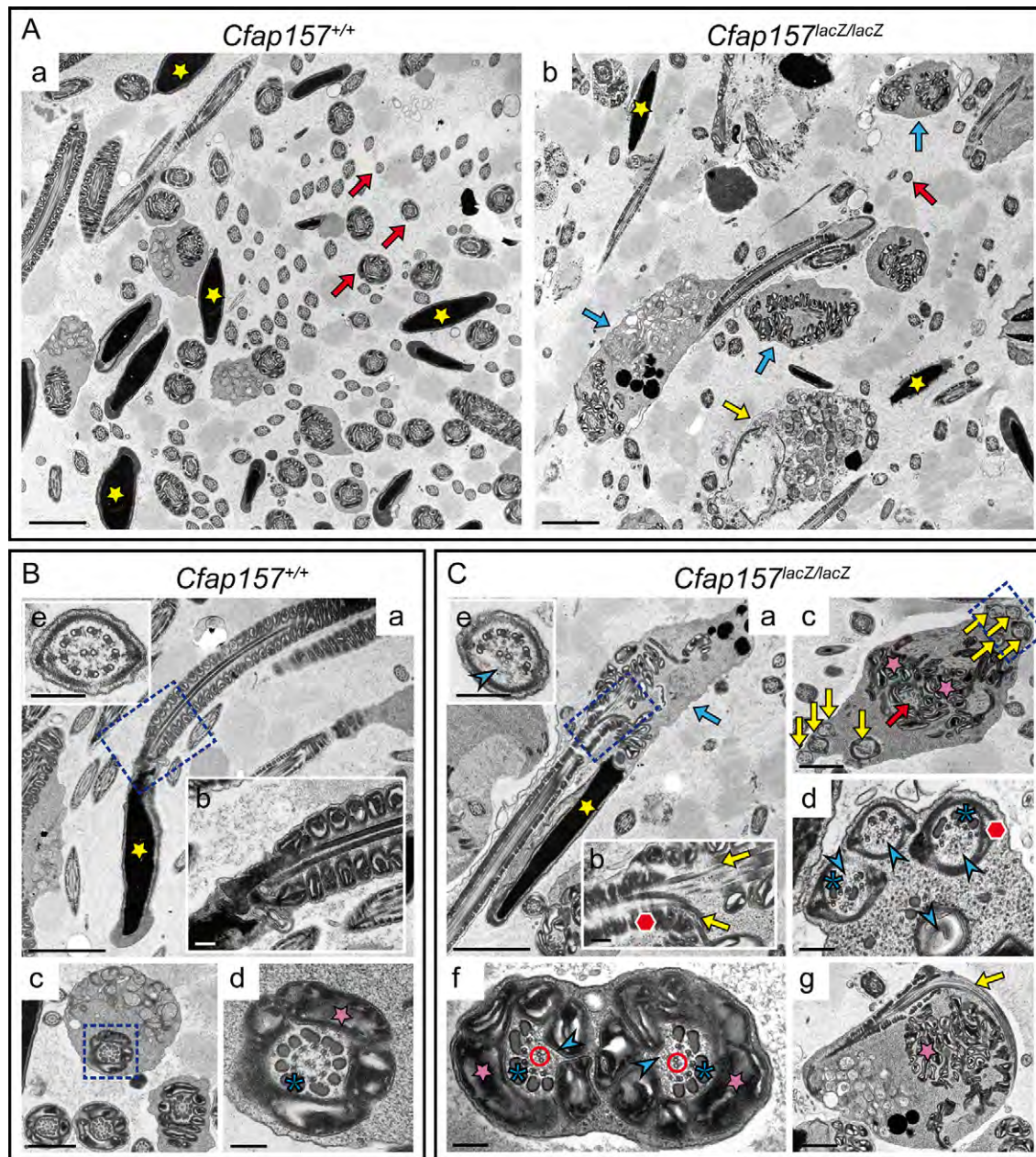
DEVELOPMENT

Fig. 9. Electron microscopy analysis of wild-type and *Cfap157^{lacZ/lacZ}* sperm in the cauda epididymis. (A) Overviews of wild-type (a) and *Cfap157^{lacZ/lacZ}* sections (b): yellow stars, sperm heads; red arrows, flagella. (B,C) Detailed images for wild type (B) and mutant (C). (a) Longitudinal section of a sperm cell: yellow stars, head; blue arrow, expanded midpiece. (b) Magnification of area boxed in a: yellow arrows, ODFs; hexagon, fibrous sheath. (c) Cross-section at the midpiece level; the wild-type section contains a cytoplasmic droplet. Red arrow indicates central axoneme; yellow arrows indicate peripheral axonemes; pink stars indicate mitochondria. (d) Magnification of the boxed area in c: pink star, mitochondria; asterisks, ODFs; blue arrowheads, missing microtubule doublets; hexagon, fibrous sheath. (e) Cross-sections of an axial filament: blue arrowhead, missing microtubule doublets. (f) Cross-section of a paired *Cfap157^{lacZ}* axoneme: pink star, mitochondria; asterisks, ODFs; blue arrowheads, missing microtubule doublets; red circles, central pairs. (g) Longitudinal section of a *Cfap157^{lacZ}* spermatozoon at the level of the axonemal loop: pink star, mitochondria. Scale bars: 2 μm in A; 2 μm in Ba,Ca; 0.2 μm in Bb,Cb; 1 μm in Bc,Cc; 0.2 μm in Bd,Cd; 0.2 μm in Be,Ce; 0.2 μm in Cf; 1 μm in Cg.

even after spermiation (Fig. 8). Formation of the sperm tail is essentially complete at spermiogenesis stage 12 (Vernet et al., 2016), preceding the alignment of mitochondria and formation of fibrous sheaths. This implies that the axonemal defects, including supernumerary axonemes develop prior to stage 12 and thus are the primary phenotype of *Cfap157*-null sperm cells. As differentiation of the sperm tail is difficult to assess in testis sections (Vernet et al., 2012), further ultrastructural analyses of testes and epididymis will clarify this issue.

Various mouse mutations that affect sperm morphology and motility have been identified (de Boer et al., 2015; reviewed by Escalier, 2006; Naz et al., 2009) but none of them resemble the *Cfap157* phenotype. Superficially, the structural defects of *Cfap157* mutant sperm showed some similarity to *Spem1*. In spermatozoa lacking *Spem1*, the midpiece wraps around the head, which is bent backwards and kept in this position by remnants of the cytoplasm (Zheng et al., 2007). *Cfap157* mutant sperm also contains excess cytoplasm; however, the axonemal loop of the midpiece appears to

be fixed by a small axonemal link that may emerge from an axonemal fork, the flagellum is not wrapped around the head, and the head is bent in smaller angles in isolated sperm. The presence of multiple flagellar axonemes in the proximal tail region and looped midpiece axonemal bundles has to the best of our knowledge not been previously described.

The localisation of CFAP157 in spermatozoa is currently unknown because we were unable to detect endogenous CFAP157 with our mouse antibodies and commercially available antibodies applying various fixation and staining protocols. Two anti-C9ORF117 antibodies produced and applied by the Human Protein Atlas both detect ciliary protein in human bronchus and nasopharynx (Ivliev et al., 2012) but show no or low diffuse cytoplasmic staining in human testis and epididymis (http://www. proteinatlas.org). This may indicate distinct localisation in different tissues or species, or be due to the inability of these antibodies to detect CFAP157 in developing spermatozoa.

Our data suggest CFAP157 localisation and function at basal bodies. An entry point into the biochemical characterisation of CFAP157 may be the validated interaction with CEP350, a centrosomal protein that binds microtubules (Hoppeler-Lebel et al., 2007; Patel et al., 2005). It controls microtubule stability and thereby plays a role in procentriole assembly, centriole elongation and Golgi organisation (Hoppeler-Lebel et al., 2007; Le Clech, 2008). Requirement of CEP350 for microtubule docking to the centrosome is controversial (Hoppeler-Lebel et al., 2007; Yan et al., 2006). CFAP157 could be involved in any of these processes. Intriguingly, CEP350 also targets proteins to the centrosome and is therefore required for ciliogenesis. An example is CYLD, a deubiquitinating enzyme that is anchored to the centrosome by CEP350, where it is required for migration and docking of basal bodies to the plasma membrane (Eguether et al., 2014).

In conclusion, we have identified a gene, *Cfap157*, that is expressed downstream of FOXJ1 in cell types carrying motile cilia with a pivotal function only in male germ cells. Our analyses suggest that CFAP157 is part of a novel mechanism that acts specifically in developing mammalian spermatozoa to ensure the formation of a single ultrastructurally correct flagellar axoneme and of a functional midpiece.

MATERIALS AND METHODS
Ethics statement, generation and husbandry of mice
Mouse and *Xenopus laevis* handling was in accordance with the German laws (Tierschutzgesetz), and was approved by the ethics committee of Lower Saxony for care and use of laboratory animals (LAVES) and by the Regional Government Stuttgart, Germany (A379/12 Zo 'Molekulare Embryologie'). Mice were housed in the animal facility of Hannover Medical School (ZTL) as approved by the responsible Veterinary Officer of the City of Hannover. Animal welfare was supervised and approved by the Institutional Animal Welfare Officer.

Cfap157^lacZneo mice were generated with EUCOMM ESC clone G05 [*1700019L03Rik^tm1a(EUCOMM)Hmgu* https://www.eummcr.org/]. Other mouse strains were Zp3:Cre (de Vries et al., 2000), FLPe (Rodríguez et al., 2000), *Foxj1⁻* (Brody et al., 2000) and CD-1 or CD-1//129/Sv hybrid as wild type. Mice were genotyped by PCR as described in the supplementary Materials and Methods.

Computer-assisted sperm analysis (CASA) and *in vitro* fertilisation (IVF)
For CASA, sperm were isolated from the cauda epididymis in 150 µl HTF medium and capacitated for 90 min at 37°C. Sperm suspension (3 µl) were analysed in a Leja Standard Count 4 Chamber Slide under an Olympus CX41 (Zuber Optik) using the QualiSperm (Biophos optimised for human sperm) software that automatically measures

motility rates and concentration of sperm. For IVF, sperm isolated from the cauda epididymis in HTF was capacitated for 2 h at 37°C and 5% CO_2. Eggs were isolated from superovulated wild-type females, incubated in HTF in groups of 40 with sperm for 6 h at 37°C under oil, washed and incubated in HTF. The presence of pronuclei was checked between 10 and 12 h after incubation with sperm. Development of blastocysts was checked after culture in KSOM from day 3.5 to 7.5 after IVF. Statistical analysis was performed using Prism (GraphPad) and one-way ANOVA.

Xenopus experiments
Xenopus microinjections, histological analyses and RNA *in situ* hybridisation were carried out essentially as described previously (Belo et al., 1997; Tingler et al., 2014). Full details are provided in the supplementary Materials and Methods.

Analysis of subcellular localisation of CFAP157-GFP in IMCD3 cells
CFAP157-GFP fusion proteins were transiently expressed in IMCD3 cells and analysed for GFP fluorescence. IMCD3 cells were also stained using acetylated and γ-tubulin. For further details, including the antibodies used, see the supplementary Materials and Methods.

Identification and validation of protein interaction partners
Tandem StrepII-Flag-tagged CFAP157 was transiently expressed in HEK293T cells and CFAP157 complexes were isolated (Gloeckner et al., 2007). Moreover, proteins from testis lysates were pulled down using purified StrepII-Flag-tagged CFAP157. Isolated CFAP157 complexes were analysed by LC-MS/MS as described previously (Boldt et al., 2011). Selected candidate interaction partners identified by MS were further analysed by co-immunoprecipitation. Details of constructs, SF-TAG purification, MS analysis and coimmunoprecipitation are provided in the supplementary Materials and Methods.

Histological methods
Immunofluorescence staining of testis sections and isolated sperm, section *in situ* hybridisation, β-galactosidase and Hematoxylin and Eosin staining were performed using standard procedures. Further details, including the antibodies used, can be found in the supplementary Materials and Methods.

Transmission electron microscopy (TEM)
Caudae epididymis and lungs were dissected from adult, 3-month-old wild-type and homozygous *Cfap157^lacZ* littermates, fixed, embedded and analysed as described previously (Rudat et al., 2014).

Southern and northern blot analysis
Southern and northern blot hybridisations were carried out according to standard procedures. Details on the probes and conditions used can be found in the supplementary Materials and Methods.

LR-PCR and (q)RT-PCR
Correct targeting of the *Cfap157* locus was confirmed by PCR on genomic DNA isolated from liver with the Expand Long Range Kit (Roche) according to the manufacturer's instructions. RT-PCR was performed on cDNA generated from total RNA isolated from various tissues of different genotypes. Details of PCR conditions, primers and fragment lengths can be found in the supplementary Materials and Methods.

Immunoprecipitation of CFAP157 from testis lysates
The generation of the monoclonal and polyclonal antibodies against CFAP157 is described in detail in the supplementary Materials and Methods. For immunoprecipitation, testes and epididymides were homogenised in 1 ml/100 mg RIPA buffer containing protease inhibitor (Roche). Lysate (500 µl) was incubated with 10 µl polyclonal antibody or monoclonal antibody 3B9 against CFAP157 for 4 h at 4°C and incubated with 20 µl prewashed protein G Sepharose (GE) overnight at 4°C. Beads were washed in RIPA buffer and resuspended in 2× sample buffer.

Precipitated proteins were detected using monoclonal antibody 3B9 (1:100) or polyclonal antibody (1:5000).

Competing interests
The authors declare no competing or financial interests.

Author contributions
M.W. designed and performed *in vivo* and *in vitro* experiments, validated knockout mice and antibodies, performed (co)immunoprecipitations, analysed data and wrote the paper; K.S.-G. established knockout mouse lines and performed *in vitro* fertilisations; M.S. participated in design and performance of some mouse experiments, analysed data and wrote the paper; C.W. and J.H. designed and performed electron microscopy, and analysed data; T.O. and M.B. designed and performed *Xenopus* experiments, and analysed data; K.B., T.B. and M.U. designed and performed tandem affinity purification and mass spectrometry, and analysed data; K.S. performed some immunoprecipitations, and stained, staged and analysed testis sections and mutant sperm; E.K. designed peptides and generated monoclonal antibodies; A.G. designed experiments, analysed data and wrote the paper; all authors read and approved the manuscript prior to submission.

Supplementary information
Supplementary information available online at
http://dev.biologists.org/lookup/doi/10.1242/dev.139626.supplemental

References
Afzelius, B. A. and Eliasson, R. (1983). Male and female infertility problems in the immotile-cilia syndrome. *Eur. J. Respir. Dis. Suppl.* **127**, 144-147.

Ahmed, E. A. and de Rooij, D. G. (2009). Staging of mouse seminiferous tubule cross-sections. *Methods Mol. Biol.* **558**, 263-277.

Alten, L., Schuster-Gossler, K., Beckers, A., Groos, S., Ulmer, B., Hegermann, J., Ochs, M. and Gossler, A. (2012). Differential regulation of node formation, nodal ciliogenesis and cilia positioning by Noto and Foxj1. *Development* **139**, 1276-1284.

Andersen, J. S., Wilkinson, C. J., Mayor, T., Mortensen, P., Nigg, E. A. and Mann, M. (2003). Proteomic characterization of the human centrosome by protein correlation profiling. *Nature* **426**, 570-574.

Banizs, B., Pike, M. M., Millican, C. L., Ferguson, W. B., Komlosi, P., Sheetz, J., Bell, P. D., Schwiebert, E. M. and Yoder, B. K. (2005). Dysfunctional cilia lead to altered ependyma and choroid plexus function, and result in the formation of hydrocephalus. *Development* **132**, 5329-5339.

Belo, J. A., Bouwmeester, T., Leyns, L., Kertesz, N., Gallo, M., Follettie, M. and De Robertis, E. M. (1997). Cerberus-like is a secreted factor with neutralizing activity expressed in the anterior primitive endoderm of the mouse gastrula. *Mech. Dev.* **68**, 45-57.

Blum, M., Schweickert, A., Vick, P., Wright, C. V. E. and Danilchik, M. V. (2014). Symmetry breakage in the vertebrate embryo: when does it happen and how does it work? *Dev. Biol.* **393**, 109-123.

Boldt, K., Mans, D. A., Won, J., van Reeuwijk, J., Vogt, A., Kinkl, N., Letteboer, S. J. F., Hicks, W. L., Hurd, R. E., Naggert, J. K. et al. (2011). Disruption of intraflagellar protein transport in photoreceptor cilia causes Leber congenital amaurosis in humans and mice. *J. Clin. Invest.* **121**, 2169-2180.

Brody, S. L., Yan, X. H., Wuerffel, M. K., Song, S.-K. and Shapiro, S. D. (2000). Ciliogenesis and left-right axis defects in forkhead factor HFH-4-null mice. *Am. J. Respir. Cell Mol. Biol.* **23**, 45-51.

Buffone, M. G., Ijiri, T. W., Cao, W., Merdiushev, T., Aghajanian, H. K. and Gerton, G. L. (2012). Heads or tails? Structural events and molecular mechanisms that promote mammalian sperm acrosomal exocytosis and motility. *Mol. Reprod. Dev.* **79**, 4-18.

Chen, J., Knowles, H. J., Hebert, J. L. and Hackett, B. P. (1998). Mutation of the mouse hepatocyte nuclear factor/forkhead homologue 4 gene results in an absence of cilia and random left-right asymmetry. *J. Clin. Invest.* **102**, 1077-1082.

Choksi, S. P., Babu, D., Lau, D., Yu, X. and Roy, S. (2014a). Systematic discovery of novel ciliary genes through functional genomics in the zebrafish. *Development* **141**, 3410-3419.

Choksi, S. P., Lauter, G., Swoboda, P. and Roy, S. (2014b). Switching on cilia: transcriptional networks regulating ciliogenesis. *Development* **141**, 1427-1441.

Cornwall, G. A. (2009). New insights into epididymal biology and function. *Hum. Reprod. Update* **15**, 213-227.

Cummins, J. M. and Woodall, P. F. (1985). On mammalian sperm dimensions. *J. Reprod. Fertil.* **75**, 153-175.

de Boer, P., de Vries, M. and Ramos, L. (2015). A mutation study of sperm head shape and motility in the mouse: lessons for the clinic. *Andrology* **3**, 174-202.

de Vries, W. N., Binns, L. T., Fancher, K. S., Dean, J., Moore, R., Kemler, R. and Knowles, B. B. (2000). Expression of Cre recombinase in mouse oocytes: a means to study maternal effect genes. *Genesis* **26**, 110-112.

Eddy, E. M. (2006). The spermatozoon. In *Knobil and Neills Physiology of Reproduction*, 3rd edn. (ed. J. D. Neill, T. M. Plant, D. W. Pfaff, J. R. G. Challi, D. M. de Kretser, J. S. Richards and P. M. Wassarman), pp. 1-52. London: Academic Press.

Eguether, T., Ermolaeva, M. A., Zhao, Y., Bonnet, M. C., Jain, A., Pasparakis, M., Courtois, G. and Tassin, A.-M. (2014). The deubiquitinating enzyme CYLD controls apical docking of basal bodies in ciliated epithelial cells. *Nat. Commun.* **5**, 4585.

Escalier, D. (2006). Knockout mouse models of sperm flagellum anomalies. *Hum. Reprod. Update* **12**, 449-461.

Fléchon, J.-E. (2016). The acrosome of eutherian mammals. *Cell Tissue Res.* **363**, 147-157.

Gerdes, J. M., Davis, E. E. and Katsanis, N. (2009). The vertebrate primary cilium in development, homeostasis, and disease. *Cell* **137**, 32-45.

Geremek, M., Bruinenberg, M., Zietkiewicz, E., Pogorzelski, A., Witt, M. and Wijmenga, C. (2011). Gene expression studies in cells from primary ciliary dyskinesia patients identify 208 potential ciliary genes. *Hum. Genet.* **129**, 283-293.

Geremek, M., Ziętkiewicz, E., Bruinenberg, M., Franke, L., Pogorzelski, A., Wijmenga, C. and Witt, M. (2014). Ciliary genes are down-regulated in bronchial tissue of primary ciliary dyskinesia patients. *PLoS ONE* **9**, e88216.

Gherman, A., Davis, E. E. and Katsanis, N. (2006). The ciliary proteome database: an integrated community resource for the genetic and functional dissection of cilia. *Nat. Genet.* **38**, 961-962.

Gloeckner, C. J., Boldt, K., Schumacher, A., Roepman, R. and Ueffing, M. (2007). A novel tandem affinity purification strategy for the efficient isolation and characterisation of native protein complexes. *Proteomics* **7**, 4228-4234.

Hall, E. A., Keighren, M., Ford, M. J., Davey, T., Jarman, A. P., Smith, L. B., Jackson, I. J. and Mill, P. (2013). Acute versus chronic loss of mammalian Azi1/Cep131 results in distinct ciliary phenotypes. *PLoS Genet.* **9**, e1003928.

Hermo, L., Pelletier, R.-M., Cyr, D. G. and Smith, C. E. (2010). Surfing the wave, cycle, life history, and genes/proteins expressed by testicular germ cells. Part 3: developmental changes in spermatid flagellum and cytoplasmic droplet and interaction of sperm with the zona pellucida and egg plasma membrane. *Microsc. Res. Tech.* **73**, 320-363.

Hoh, R. A., Stowe, T. R., Turk, E. and Stearns, T. (2012). Transcriptional program of ciliated epithelial cells reveals new cilium and centrosome components and links to human disease. *PLoS ONE* **7**, e52166.

Hoppeler-Lebel, A., Celati, C., Bellett, G., Mogensen, M. M., Klein-Hitpass, L., Bornens, M. and Tassin, A.-M. (2007). Centrosomal CAP350 protein stabilises microtubules associated with the Golgi complex. *J. Cell Sci.* **120**, 3299-3308.

Irons, M. J. and Clermont, Y. (1982). Kinetics of fibrous sheath formation in the rat spermatid. *Am. J. Anat.* **165**, 121-130.

Ivliev, A. E., 't Hoen, P. A. C., van Roon-Mom, W. M. C., Peters, D. J. M. and Sergeeva, M. G. (2012). Exploring the transcriptome of ciliated cells using in silico dissection of human tissues. *PLoS ONE* **7**, e35618.

Jacquet, B. V., Salinas-Mondragon, R., Liang, H., Therit, B., Buie, J. D., Dykstra, M., Campbell, K., Ostrowski, L. E., Brody, S. L. and Ghashghaei, H. T. (2009). FoxJ1-dependent gene expression is required for differentiation of radial glia into ependymal cells and a subset of astrocytes in the postnatal brain. *Development* **136**, 4021-4031.

Jain, R., Pan, J., Driscoll, J. A., Wisner, J. W., Huang, T., Gunsten, S. P., You, Y. and Brody, S. L. (2010). Temporal relationship between primary and motile ciliogenesis in airway epithelial cells. *Am. J. Respir. Cell Mol. Biol.* **43**, 731-739.

Kleene, K. C. (2005). Sexual selection, genetic conflict, selfish genes, and the atypical patterns of gene expression in spermatogenic cells. *Dev. Biol.* **277**, 16-26.

Le Clech, M. (2008). Role of CAP350 in centriolar tubule stability and centriole assembly. *PLoS ONE* **3**, e3855.

Lee, L. (2013). Riding the wave of ependymal cilia: genetic susceptibility to hydrocephalus in primary ciliary dyskinesia. *J. Neurosci. Res.* **91**, 1117-1132.

Li, W., Park, J. Y., Zheng, D., Hoque, M., Yehia, G. and Tian, B. (2016). Alternative cleavage and polyadenylation in spermatogenesis connects chromatin regulation with post-transcriptional control. *BMC Biol.* **14**, 6.

Lyons, R. A., Saridogan, E. and Djahanbakhch, O. (2006). The reproductive significance of human fallopian tube cilia. *Hum. Reprod. Update* **12**, 363-372.

McClintock, T. S., Glasser, C. E., Bose, S. C. and Bergman, D. A. (2008). Tissue expression patterns identify mouse cilia genes. *Physiol. Genomics* **32**, 198-206.

Meistrich, M. L. and Hess, R. A. (2013). Assessment of spermatogenesis through staging of seminiferous tubules. *Methods Mol. Biol.* **927**, 299-307.

Naz, R. K., Engle, A. and None, R. (2009). Gene knockouts that affect male fertility: novel targets for contraception. *Front. Biosci.* **14**, 3994-4007.

Nigg, E. A. and Raff, J. W. (2009). Centrioles, centrosomes, and cilia in health and disease. *Cell* **139**, 663-678.

Nonaka, S., Tanaka, Y., Okada, Y., Takeda, S., Harada, A., Kanai, Y., Kido, M. and Hirokawa, N. (1998). Randomization of left-right asymmetry due to loss of nodal cilia generating leftward flow of extraembryonic fluid in mice lacking KIF3B motor protein. *Cell* **95**, 829-837.

Patel, H., Truant, R., Rachubinski, R. A. and Capone, J. P. (2005). Activity and subcellular compartmentalization of peroxisome proliferator-activated receptor alpha are altered by the centrosome-associated protein CAP350. *J. Cell Sci.* **118**, 175-186.

Praveen, K., Davis, E. E. and Katsanis, N. (2015). Unique among ciliopathies: primary ciliary dyskinesia, a motile cilia disorder. *F1000Prime Rep.* **7**, 36.

Rodríguez, C. I., Buchholz, F., Galloway, J., Sequerra, R., Kasper, J., Ayala, R., Stewart, A. F. and Dymecki, S. M. (2000). High-efficiency deleter mice show that FLPe is an alternative to Cre-loxP. *Nat. Genet.* **25**, 139-140.

Rossi, A., Kontarakis, Z., Gerri, C., Nolte, H., Hölper, S., Krüger, M. and Stainier, D. Y. R. (2015). Genetic compensation induced by deleterious mutations but not gene knockdowns. *Nature* **524**, 230-233.

Rudat, C., Grieskamp, T., Röhr, C., Airik, R., Wrede, C., Hegermann, J., Herrmann, B. G., Schuster-Gossler, K. and Kispert, A. (2014). Upk3b is dispensable for development and integrity of urothelium and mesothelium. *PLoS ONE* **9**, e112112.

Sakai, Y., Koyama, Y.-I., Fujimoto, H., Nakamoto, T. and Yamashina, S. (1986). Immunocytochemical study on fibrous sheath formation in mouse spermiogenesis using a monoclonal antibody. *Anat. Rec.* **215**, 119-126.

Santos, N. and Reiter, J. F. (2008). Building it up and taking it down: the regulation of vertebrate ciliogenesis. *Dev. Dyn.* **237**, 1972-1981.

Schürmann, A., Koling, S., Jacobs, S., Saftig, P., Krauss, S., Wennemuth, G., Kluge, R. and Joost, H.-G. (2002). Reduced sperm count and normal fertility in male mice with targeted disruption of the ADP-ribosylation factor-like 4 (Arl4) gene. *Mol. Cell. Biol.* **22**, 2761-2768.

Sironen, A., Kotaja, N., Mulhern, H., Wyatt, T. A., Sisson, J. H., Pavlik, J. A., Miiluniemi, M., Fleming, M. D. and Lee, L. (2011). Loss of SPEF2 function in mice results in spermatogenesis defects and primary ciliary dyskinesia. *Biol. Reprod.* **85**, 690-701.

Skerget, S., Rosenow, M. A., Petritis, K. and Karr, T. L. (2015). Sperm proteome maturation in the mouse epididymis. *PLoS ONE* **10**, e0140650.

Spassky, N., Merkle, F. T., Flames, N., Tramontin, A. D., García-Verdugo, J. M. and Alvarez-Buylla, A. (2005). Adult ependymal cells are postmitotic and are derived from radial glial cells during embryogenesis. *J. Neurosci.* **25**, 10-18.

Stannard, W. and O'Callaghan, C. (2006). Ciliary function and the role of cilia in clearance. *J. Aerosol. Med.* **19**, 110-115.

Stauber, M., Weidemann, M., Dittrich-Breiholz, O., Lobschat, K., Alten, L., Mai, M., Beckers, A., Kracht, M. and Gossler, A. (2016). Identification of FOXJ1 effectors during ciliogenesis in the foetal respiratory epithelium and embryonic left-right organiser of the mouse. *Dev. Biol.* (in press).

Stubbs, J. L., Oishi, I., Izpisúa Belmonte, J. C. and Kintner, C. (2008). The forkhead protein Foxj1 specifies node-like cilia in Xenopus and zebrafish embryos. *Nat. Genet.* **40**, 1454-1460.

Takeda, S., Yonekawa, Y., Tanaka, Y., Okada, Y., Nonaka, S. and Hirokawa, N. (1999). Left-right asymmetry and kinesin superfamily protein KIF3A: new insights in determination of laterality and mesoderm induction by kif3A-/- mice analysis. *J. Cell Biol.* **145**, 825-836.

Tingler, M., Ott, T., Tözser, J., Kurz, S., Getwan, M., Tisler, M., Schweickert, A. and Blum, M. (2014). Symmetry breakage in the frog Xenopus: role of Rab11 and the ventral-right blastomere. *Genesis* **52**, 588-599.

Vernet, N., Mahadevaiah, S. K., Ellis, P. J. I., de Rooij, D. G. and Burgoyne, P. S. (2012). Spermatid development in XO male mice with varying Y chromosome short-arm gene content: evidence for a Y gene controlling the initiation of sperm morphogenesis. *Reproduction* **144**, 433-445.

Vernet, N., Mahadevaiah, S. K., Decarpentrie, F., Longepied, G., de Rooij, D. G., Burgoyne, P. S. and Mitchell, M. J. (2016). Mouse Y-encoded transcription factor Zfy2 is essential for sperm head remodelling and sperm tail development. *PLoS ONE* **11**, e0145398.

Vij, S., Rink, J. C., Ho, H. K., Babu, D., Eitel, M., Narasimhan, V., Tiku, V., Westbrook, J., Schierwater, B. and Roy, S. (2012). Evolutionarily ancient association of the FoxJ1 transcription factor with the motile ciliogenic program. *PLoS Genet.* **8**, e1003019.

Yan, X., Habedanck, R. and Nigg, E. A. (2006). A complex of two centrosomal proteins, CAP350 and FOP, cooperates with EB1 in microtubule anchoring. *Mol. Biol. Cell* **17**, 634-644.

Yániz, J. L., Soler, C. and Santolaria, P. (2015). Computer assisted sperm morphometry in mammals: a review. *Anim. Reprod. Sci.* **156**, 1-12.

Yu, X., Ng, C. P., Habacher, H. and Roy, S. (2008). Foxj1 transcription factors are master regulators of the motile ciliogenic program. *Nat. Genet.* **40**, 1445-1453.

Zhang, Y., Ou, Y., Cheng, M., Saadi, H. S., Thundathil, J. C. and van der Hoorn, F. A. (2012). KLC3 is involved in sperm tail midpiece formation and sperm function. *Dev. Biol.* **366**, 101-110.

Zheng, H., Stratton, C. J., Morozumi, K., Jin, J., Yanagimachi, R. and Yan, W. (2007). Lack of Spem1 causes aberrant cytoplasm removal, sperm deformation, and male infertility. *Proc. Natl. Acad. Sci. USA* **104**, 6852-6857.

DEVELOPMENT